Multinode Bilateral Control Model

Liang Wang and Berthold K. P. Horn

***Abstract*—Bilateral control can suppress traffic flow instabilities. The simplest form of bilateral control uses information about the relative positions and relative velocities of leading and trailing vehicles. In this paper, we provide a multinode version of bilateral control, in which information about the state of more than just the immediately leading and trailing cars is used. In this mode of control, the question arises: "How much weight should information about vehicles at different positions be given?" Two different methods—a Taylor series approach and a least-squares approach—are explored. We show that the least-squares approach generates sets of coefficients that can damp out low-frequency components of perturbations faster. This means that traffic under multinode bilateral control will approach an equilibrium state more rapidly than under the traditional version of bilateral control. Simulation results confirm our analysis.**

***Index Terms*—Bilateral control, Fourier analysis, least-squares approximation, Taylor series, traffic flow instabilities.**

I. Introduction and Related Work

With the rapid development of sensors and wireless communications, driver assistance systems and self-driving cars come closer and closer to reality. Such systems can take into account more information about the environment of the car than a human driver, e.g., the distances between the current car and the following car. By using this additional information cleverly, new control strategies can be used to solve traffic flow problems caused by the car-following behavior of human drivers.

One basic question is whether control should be organized primarily locally (by focusing on controlling a single car) or primarily globally (by focusing on controlling a whole line of traffic). Based on different answers to this question, the following two types of models have been proposed.

1) *Local control strategy:* "control of that car, by that car and for that car!" A representative model is known as *bilateral control* [1]–[4]. The state (i.e., position and speed) of the current car is controlled to match the average state of the leading and following cars. In this model, there are *no* "lead vehicles," nor global communication. The control of each car in the traffic is based *only* on the states of its neighbors. (For other efforts involving use of bidirectional information flow, see [5]–[7].)
2) *Global control strategy:* "controlling the whole line of traffic to move like a train!" A representative model is known as the *platoon* [8]–[12]. Closer to our interests here is a particular extension of this, namely the *bidirectional platoon* [14]–[17]. See [13], [18]–[21], [25]–[30] for more theoretical analyses of various platoon models, e.g., the string stability conditions for one-directional platooning (i.e., predecessor following control architecture) [25], [26], [30] and the stability analysis of bidirectional platooning [13]. Basically, the performance of a platoon can be increased greatly by adding information about the following cars [13]–[15]. The leading vehicle (whose state is communicated wirelessly to all of the following vehicles) controls all of the cars in the platoon. All of the information is transmitted by global communication.[1]

Bilateral control is *different* from platoon control. Platoon control is a method of controlling a whole string of vehicles, whereas bilateral control is a strategy for controlling individual cars separately. Bilateral control can be thought of as a new type of adaptive cruise control (ACC) mode (which can be built in the car during the manufacturing process). In this case, of course, it is not known ahead of time what role the car will play—whether the car will be the first in a string of cars, or the last car, or one of the cars in between. In contrast, platoon control is a method of putting successive vehicles together, where each car knows the role it plays in the platoon, e.g., its index in the vehicular string. For a platoon controller, the objective is generally to stay at a desired relative position in the vehicular platoon. For bilateral control, the control goal is simply to be in the middle between its immediate neighbors (i.e., as far from the leading car as from the following car). In fact, bilateral control is an extension of the traditional "car-following" model with information about the following car added. Note also that the following conditions hold.

1) Bilateral control does not try to bind successive cars together to force them to move in lock-step like carriages in a train, which is exactly what platooning does. The

Manuscript received February 3, 2018; revised September 11, 2018; accepted December 8, 2018. Date of publication January 9, 2019; date of current version September 25, 2019. This work was supported by Toyota Research Institute under Grant LP-C000765-SR. Recommended by Associate Editor F. R. Wirth. *(Corresponding author: Berthold K. P. Horn.)*

L. Wang is with the Computer Science and Artificial Intelligence Laboratory, Massachusetts Institute of Technology, Cambridge, MA 02139 USA (e-mail: wangliang@csail.mit.edu).

B. K. P. Horn is with the Department of Electrical Engineering and Computer Science, Massachusetts Institute of Technology, Cambridge, MA 02139 USA (e-mail: bkph@csail.mit.edu).

Color versions of one or more of the figures in this paper are available online at http://ieeexplore.ieee.org.

Digital Object Identifier 10.1109/TAC.2019.2891490

[1]Some platoon models use a preset desired speed (in general, the speed of the lead vehicle) to control the cars [14], [15]. Even if the speed of the lead car is constant most of the time, in order to guarantee safety, the state of the lead car must be broadcast to all cars in the platoon continuously. Thus, global communication is needed in general.

vehicles in traffic under bilateral control still act like cars, rather than tied-together "carriages" of a train. There is *no* "locomotive" as there is for controlling a whole platoon. Moreover, wireless communication is *not* necessary for bilateral control. Control action can be computed based on the measurements obtained by on-board sensors alone. Acceleration of neighboring cars—which is used in recent advanced platoon models [32]–[36]—is not used in bilateral control. Acceleration information would have to be shared through wireless communication. More importantly, cars under bilateral control are relatively independent. The control system (and control information) is not available to other cars.

2) Bilateral control is more practical and flexible than platooning because it can be used in mixed traffic situations. Although there are some studies on merge control of platooning [22]–[24], the merged cars become new lock-step "carriages," rather than independent vehicles. In real application, gaps between cars in a platoon are controlled to be small on purpose, which prevents other vehicles from merging in. Under bilateral control, cars are allowed to merge into (or extricate themselves from) the traffic flow independently (see [4, Fig. 6]).
3) Bilateral control does not exclude wireless communication between cars. It has been shown, for example, that adding intervehicle communication to sensor information makes a system under bilateral control robust against various types of failures, such as failures of individual sensors or individual communication links [2]. Also, information about neighboring vehicles obtained using communication can be used for fusion with the measurement from the vehicle's own sensors.

Perhaps we can have the best of both worlds by using information from both sensors and (local) wireless communication. This raises new issues, such as "How to fuse information from sensors and (local) wireless communication?" Perhaps an even more interesting question is "How to use this information best?" Correspondingly, the bilateral control strategy is here extended to a multinode bilateral control model (MN-BCM), which uses information about more than just the immediately leading and following cars. Information about other nearby cars is obtained by wireless communication. The basic strategy of multinode bilateral control is based on the philosophy of bilateral control in [1]: control is distributed, there is no "leader" or central node of control, the control system (including control commands) is not accessible to control systems in other cars.

In simple bilateral control, equal weight is given to information about the relative positions and relative velocities of the leading and trailing cars. This constrains the weights used in the control algorithm. When we have information about additional nearby cars, we have more degrees of freedom and need to come up with a reasonable scheme for picking weights. We explore two methods of generating "optimal" coefficients for multinode bilateral control—the Taylor series approach and the least-squares approach. These appear to be two natural ways of extending the BCM in [1].

We give detailed analysis of these approaches, and provide several possible schemes for the implementation of multinode bilateral control. For the Taylor series approach, the best result that can be obtained is from approximation of the second-order polynomial in the frequency domain. For the least-squares approach, the situation is more flexible. For example, we can try to approximate a functions with higher decay rate when the frequency is small, e.g., the absolute-value function. Correspondingly, such solutions can damp low-frequency waves of perturbation much faster than those obtained by approximating the second-order polynomial.

The rest of this paper is organized as follows. Section II reviews the (simplest) BCM, and the stability of BCM. Section III describes the MN-BCM, and the stability analysis of MN-BCM. We go on to provide two approaches, i.e., Taylor series approach and least-squares approaches, of generating the coefficients. We show that: 1) Taylor series approach is limited, and 2) least-squares approach can generate sets of coefficients that damp out low-frequency components of perturbations faster. Section IV provides one sufficient condition (see Theorem 3) and one necessary condition (see Theorem 4) for testing stability of MN-BCM. We prove that all the MN-BCMs proposed in this paper are stable. Theorems 3 and 4 can then be used to check the newly designed MN-BCMs. Section V provides several simulations to test various MN-BCMs proposed in this paper. Finally, Section VI concludes the paper with possible extension of MN-BCM for more general settings.

II. Bilateral Control Revisited

Let $x_n(t)$ be the position of the nth car, and $v_n(t) = \dot{x}_n(t)$ its velocity.[2] The state of the nth car—denoted by $\{x_n(t), v_n(t)\}$—is adjusted through the acceleration $a_n(t) = \ddot{x}_n(t)$ commanded by the control system. For the BCM [1]

$$a_n = k_d\left(x_{n-1} - 2x_n + x_{n+1}\right) + k_v\left(v_{n-1} - 2v_n + v_{n+1}\right). \tag{1}$$

In consideration of passengers' comfort, in general, the two gains $k_d > 0$ and $k_v > 0$ are chosen to be relatively small (positive) numbers. Note that control of car n is based on the relative positions and relative velocities of *both* car $(n-1)$ ahead and car $(n+1)$ behind [see Fig. 1(a)]. Only distance sensors $d_n = x_{n-1} - x_n - L$ (with car length as L) and speed difference sensors $r_n = v_{n-1} - v_n$ are needed to implement bilateral control, i.e.,

$$a_n = k_d\left(d_n - d_{n+1}\right) + k_v\left(r_n - r_{n+1}\right). \tag{2}$$

For car n, the distance measurement d_n and d_{n+1} can come from two sensors mounted fore and aft on car n. None of this requires vehicle-to-vehicle (V2V) communication. However, if we *do* have V2V available, then we can potentially halve the number of sensors required overall, since vehicle n need only measure d_n and r_n using its own sensors, and obtain d_{n+1} and r_{n+1} from sensors mounted on car $(n+1)$. If, on the other

[2]Note that x_{n-1} and x_n denote the position of the leading car and the current car, respectively. The positive direction is the direction in which the cars are moving, thus, $x_{n-1} - x_n > 0$ (see Fig. 1).

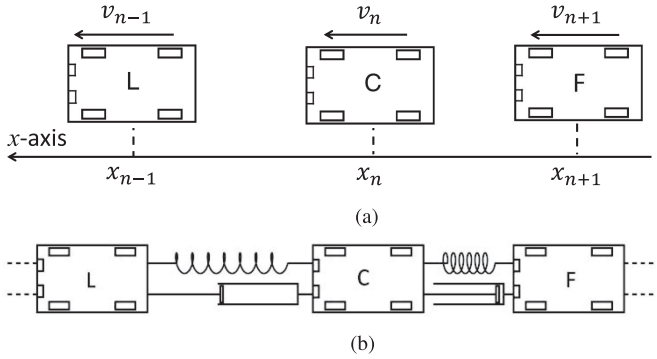

Fig. 1. Illustration of the BCM. The blocks marked "L," "C," and "F" denote the leading car, current car, and following car, respectively. (a) State of the current car is controlled to match the *average* state of the leading car "L" and following car "F." (b) Physical analog of the traffic flow under bilateral control is a big "spring-mass-damper" system.

hand, such a system does have a full set of sensors, then V2V will make it more reliable. In particular, if some sensors on car n fail, then it can get the required measurements from car $(n+1)$ or car $(n-1)$.

A physical analog of a line of traffic under bilateral control (2) is a big "spring-mass-damper" system [see Fig. 1(b)]. Intuitively, a perturbation will lead to damped waves travelling outward in both directions from the point of perturbation. The amplitude of these waves decays as they travel, so traffic flow under bilateral control is *stable*.[3] See [1] and [4] for the detailed analysis and the control system implementation.

Bilateral control is stable for all $k_d > 0$ and $k_v > 0$ [1], [3], [4]. One way of demonstrating the stability is to replace the mixed continuous/discrete ordinary differential equations (ODEs) (1) with the continuous partial differential equation (PDE)

$$\frac{\partial^2 x}{\partial t^2} - k_v \frac{\partial^2}{\partial n^2}\left(\frac{\partial x}{\partial t}\right) - k_d \frac{\partial^2 x}{\partial n^2} = 0 \tag{3}$$

and show that all the nonzero frequency components of the traveling wave will be damped [4]. Here, the function $x(n,t)$ in (3) is the continuous analog of the vector $\mathbf{x}(t) = (\ldots, x_{n-1}(t), x_n(t), x_{n+1}(t), \ldots)^T$. The analysis of the case of the finite vector $(x_1(t), \ldots, x_k(t), \ldots, x_N(t))^T$ can be found in [3]. The paper presented in [3] also shows the proof that bilateral control suppresses traffic instabilities under any and all of the various boundary conditions: circular boundaries, fixed–fixed boundaries, free–free boundaries, and fixed–free boundaries. In general, free–free boundaries are used in bilateral control.[4]

[3]Note that "stability" does not imply that there is a guarantee that there will be no collisions. Stability means that any perturbation from the equilibrium state will be damped out and eventually disappear. It is possible that—during the decay of propagating waves caused by a large enough perturbation—vehicle trajectories may cross. This is similar to the situation with "string stability" [27]–[30], which does not guarantee freedom from collisions. In the case of bilateral control, constraints on the initial conditions *can* provide guarantees of no collisions, but that is the subject of another paper.

[4]Different from platooning—whose boundaries are used to control the desired states of all vehicles in the platoon—bilateral control only focuses on the control of a single car. The boundary condition in bilateral control is just used to design the ACC system, e.g., by setting thresholds of measurement from range sensors, such that the car can operate on the road alone.

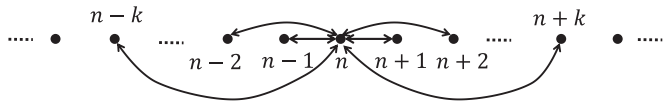

Fig. 2. Multinode bilateral control. Each node denotes a vehicle in the line of traffic. Information about all $2k$ neighboring cars is used to control the state of the current car.

Moreover, the first and last cars (i.e., boundaries) can move independently, e.g., human drivers, in which case their states are treated as part of the input to the system.

Decentralized control has been well-studied in platooning [12]–[16]. Some decentralized platoon models attempt not to use preset desired speed [37]–[41]. Still, (preset) desired spacing is used in platooning, and the lead vehicle plays an important role (explicitly or implicitly) in general to control the vehicles. In bilateral control, there is no lead vehicle, or preset desired speed, or preset desired spacing.

Bilateral control uses the relative velocity between neighboring cars as the additional feedback control. Here, we should mention that the relative velocity based feedback component, i.e., the "dampers" in Fig. 1(b), is *necessary*. Otherwise, as mentioned in [13], error amplification might break stability and cause traffic jam or car collisions.

III. Multinode Bilateral Control

Bilateral control can be implemented without using wireless communication. However, if V2V is available, additional measurements from neighboring cars can be used for fusion with measurements from on-board sensors, and the system becomes more reliable—being able to adjust to failures of individual sensors. In addition, more information can be obtained using wireless communication. For instance, instead of information only about the two directly adjacent cars, the states of say $2k$ neighboring cars can be obtained and potentially be used in control. How to use the information about (or from) these $2k+1$ cars (also called $2k+1$ nodes) is the central problem studied in this paper.

We can use a feedback control strategy similar to that of the simple bilateral control (1), except that now information about the state of $2k+1$ nodes (for $k > 1$) is used as input rather than just 3. That is,

$$a_n = k_d \left(\sum_{m=-k}^{k} g_m x_{n-m} \right) + k_v \left(\sum_{m=-k}^{k} h_m v_{n-m} \right). \tag{4}$$

Here, $\{g_m\}$ and $\{h_m\}$ are sets of coefficients (with $2k+1$ entries) as yet to be determined. Equation (4) is called the MN-BCM (or $2k+1$ node) in this paper (see Fig. 2). Traditional bilateral control (1) is a 3-node model with both $\{g_m\}$ and $\{h_m\}$ equal to $\{1, -2, 1\}$.

Similar to (2), i.e., the implementation of the simplest bilateral control, the MN-BCM (4) can be implemented by

$$a_n = k_d \left(\sum_{m=-k}^{k-1} \alpha_m d_{n-m} \right) + k_v \left(\sum_{m=-k}^{k-1} \beta_m r_{n-m} \right). \tag{5}$$

That is, local measurements are shared among neighboring cars through V2V. Overall, $2k$ space measurements and $2k$ relative speed measurements are used for control, and $\{\alpha_m\}$ and $\{\beta_m\}$ in (5) are the weights for each measurement. In distinction to platoon models [32]–[37], *no* desired relative positions (i.e., desired spacing) or acceleration information of neighboring cars are used for control in MN-BCM.

Comparing (4) and (5), we find that

$$\alpha_{k-l-1} = \sum_{m=0}^{l} g_{k-m} \quad \text{and} \quad \beta_{k-l-1} = \sum_{m=0}^{l} h_{k-m} \tag{6}$$

for $l = 0, 1, 2, \ldots, 2k-1$. The next question is how to pick suitable coefficients $\{g_m\}$ and $\{h_m\}$ in (4) [or equivalent the coefficients $\{\alpha_m\}$ and $\{\beta_m\}$ in (5)]. Here, we should mention that similar topological structure to Fig. 2 has been used by existing platoon models [33], [35], [37]. However, the studies of how to determine the coefficients $\{g_m\}$ and $\{h_m\}$ proposed in this paper have not been explored in those platoon models.

A. Stability Analysis

For simplicity, we only consider the case that $g_m = h_m$ (for all $m = -k, \ldots, k$), and all the coefficients $\{g_m\}$ are *real* numbers. In this paper, stability means the following.

Definition 1: If the traffic flow under multinode bilateral control goes to the *equilibrium state*, in which cars are equally spaced and all move at the same speed, from arbitrary initial state (as $t \to \infty$), then we call the MC-BCM stable.

The system (4) is linear and shift invariant [43]. Thus, its response to a single-frequency wave, i.e., $x_n(0) = e^{-in\omega}$, is the same frequency wave whose magnitude (and phase) is $p_\omega(t)$, i.e., $x_n(t) = e^{-in\omega} p_\omega(t)$. Substituting $x_n(t) = e^{-in\omega} p_\omega(t)$ into (4), we find

$$\ddot{p}_\omega(t) - k_v f(\omega) \dot{p}_\omega(t) - k_d f(\omega) p_\omega(t) = 0 \tag{7}$$

where $f(\omega)$ is also called the *discrete-time Fourier transform* of the coefficients $\{g_m\}$, i.e.,

$$f(\omega) = \sum_{m=-k}^{k} g_m e^{im\omega}. \tag{8}$$

The solution of the ODE (7) is[5] [43]

$$p_\omega(t) = b_1 e^{s_1(\omega)t} + b_2 e^{s_2(\omega)t} \tag{9}$$

where b_1 and b_2 are two constants (determined by the initial conditions), and s_1 and s_2 satisfy

$$s_1 + s_2 = k_v f(\omega) \quad \text{and} \quad s_1 s_2 = -k_d f(\omega). \tag{10}$$

The stability in Definition 1 requires $p_\omega(t) \to 0$ as $t \to \infty$ for all $0 < |\omega| \le \pi$. That is, both $s_1(\omega)$ and $s_2(\omega)$ should have negative real part. Note that if $f(\omega)$ is a real function, then the stability condition is $f(\omega) < 0$ for all $0 < |\omega| \le \pi$ [see (10)]. Thus, one simple choice is letting $f(\omega)$ be a negative even function[6] for all $0 < |\omega| \le \pi$.

Now we can understand the reason that the PDE (3) is stable. The corresponding $f(\omega) = -\omega^2$ is negative when $\omega \neq 0$. The BCM (1) uses the three-point scheme with coefficients $\{1, -2, 1\}$ to approximate the second derivative, and the corresponding $f(\omega) = -4\sin^2(\omega/2)$ is also negative. Thus, the traffic flow under bilateral control (1) is also stable.

Note that the equilibrium state $x_n(t) = X + n\,s + V\,t$ should be a solution of the MN-BCM (4), where X is the position of the first car, s is the (equal) position difference between cars, and V is the velocity of all cars. Thus, we find the following two additional constraints:

$$\sum_{m=-k}^{k} g_m = 0 \quad \text{and} \quad \sum_{m=-k}^{k} g_m m = 0. \tag{11}$$

The first equation in (11) implies that $f(0) = 0$. The second equation in (11) will be automatically satisfied if the coefficients $\{g_m\}$ are *symmetric* (i.e., $g_m = g_{-m}$), which implies that $f(\omega)$ is a real (and even) function. In summary, we have proven the following theorem.

Theorem 1: The symmetric multinode bilateral control (i.e., $g_m = g_{-m}$) is stable if and only if $\{g_m\}$ in (8) satisfy 1) $f(\omega) < 0$ (for all $0 < |\omega| \le \pi$) and 2) $f(0) = 0$.

The choice of symmetric weights $\{g_m\}$ is sufficient but not necessary for the conditions in (11). That is, the choice of asymmetric weights is not excluded by (11). Bilateral control is a new cruise control mode used by self-driving (or sensors based) cars. For such cars, looking back is no different than looking forward. Thus, information from the rear and front sensors can be treated equally. In some traffic models of platooning or human drivers, nonsymmetric weights might be a better choice [5], [14], [32]–[38]. As an extension of the original BCM, we focus on symmetric weights in this paper.

B. Generating the Coefficients

The stability condition in Theorem 1 still leaves a lot of degrees of freedom. For instance, $f(\omega)$ could approximate the (negative) even order powers of ω, i.e., $-\omega^2$, or $-\omega^4$, or $-\omega^6$, . . ., and their linear combinations.[7] When $|\omega|$ is small (and thus $|f(\omega)|$ is also small), the real part of the two roots s_1 and s_2 is both $\frac{1}{2}k_v f(\omega)$ [see (10)]. Thus, the smaller the $f(\omega)$ is (when $|\omega|$ is small), the faster the $p_\omega(t)$ in (9) goes to zero. Roughly speaking, the objective of optimizing $\{g_m\}$ in (8) is to "make $f(\omega)$ as small as possible (or equivalently $|f(\omega)|$ as large as possible) when $|\omega|$ is small" subject to the stability constraints in Theorem 1. Near $\omega = 0$, the smallest possible value of (minus) even powers of ω is attained when $f(\omega)$ is a multiple of $-\omega^2$. Thus, one possible approach is to approximate $-\omega^2$ using *Taylor series*.

[5]Here, we suppose that $f(\omega) \neq 0$. If $f(\omega) = 0$, then (7) becomes $\ddot{p}_\omega(t) = 0$, and then the general solution is $p_\omega(t) = b_1 + b_2 t$. Thus, $|p_\omega(t)|$ can be unbounded and the system is unstable.

[6]From the definition of $f(\omega)$ [in (8)], we can see that if $f(\omega)$ is a real function, then it must be an even function. Moreover, $f(\omega)$ in (8) is a periodic function. Thus, we need only consider the region $-\pi \le \omega \le \pi$.

[7]Note that the lowest-order polynomial that can be used here is $-\omega^2$, rather than the negative constant (i.e., $-\omega^0$, the zeroth order) since $f(0) = 0$.

1) Taylor Series Approach: The Taylor series of $f(\omega)$ is

$$\left(\sum_{m=-k}^{k} g_m\right) + \left(\sum_{m=-k}^{k} g_m m\right) i\omega - \left(\sum_{m=-k}^{k} g_m m^2\right)\frac{\omega^2}{2} - \left(\sum_{m=-k}^{k} g_m m^3\right)\frac{i\omega^3}{3!} + \left(\sum_{m=-k}^{k} g_m m^4\right)\frac{\omega^4}{4!} + \cdots . \tag{12}$$

The first $2k+1$ coefficients of the Taylor series of $-\omega^2$ are $\mathbf{b} = (0, 0, -1, 0, 0, \ldots, 0)^T$. Thus, matching the coefficients of the Taylor series gives the following linear equation:

$$\mathbf{F}\mathbf{g} = -2\mathbf{b} \tag{13}$$

where $\mathbf{F}$ is exactly the transpose of the $(2k+1)\times(2k+1)$ *Vandermonde matrix* [42]. That is, the element in row i and column j of $\mathbf{F}$ is $(j-k-1)^{i-1}$. The coefficients $\mathbf{g} = (g_{-k}, \ldots, g_0, g_1, \ldots, g_k)^T$ can be found using $\mathbf{g} = -2\mathbf{F}^{-1}\mathbf{b}$, i.e., the third column of the matrix $2\mathbf{F}^{-1}$.

The solution when $k=1$ is $\mathbf{g} = (1, -2, 1)^T$, which is exactly the set of coefficients used by the simplest BCM (1). The explicit form of the entries in $\mathbf{F}^{-1}$ is well known [44], [45]. Thus, the coefficients $\{g_m\}$ can be calculated directly. For instance, the coefficients are $\{-1/12,\ 4/3,\ -5/2,\ 4/3,\ -1/12\}$ when $k=2$, and the coefficients are $\{1/90,\ -3/20,\ 3/2,\ -49/18,\ 3/2, -3/20, 1/90\}$ when $k=3$. The contributions from distant cars are much smaller than those from immediate neighbors.

Fig. 3 shows the curves of $f(\omega)$ when $k=1,2,3$. As a comparison, we also show the curve (in red) when $\{g_m\}$ is chosen as $\{-1,\ 4,\ -6,\ 4,\ -1\}$, that is, the Taylor series matching result of the fourth-order polynomial $-\omega^4$. The corresponding $|f(\omega)|$ is much smaller when $|\omega|$ is small [see Fig. 3(b)]. Thus, the low-frequency waves will be damped much more slowly when using the fourth-order coefficients $\{-1,\ 4,\ -6,\ 4,\ -1\}$ (compared to the second-order scheme $\{-1/12,\ 4/3,\ -5/2,\ 4/3,\ -1/12\}$). The first two equations in (13) imply that the conditions in (11) are satisfied. All the even rows in (13) form (in total k) linear equations with k unknowns, i.e., $\sum_{m=1}^{k} m^{2n-1}(g_m - g_{-m}) = 0$ for $n = 1, 2, \ldots, k$. The solution is $g_m - g_{-m} = 0$ (or $g_m = g_{-m}$) for all $m = 1, 2, \ldots, k$. Thus, the coefficients $\{g_m\}$ *are* symmetric.

2) Least-Squares Approach: Note that not all functions (e.g., $-|\omega|$) have Taylor series expansion (at $\omega = 0$). We can also try to determine the coefficients $\{g_m\}$ by other optimization methods. For instance, to match some objective function $z(\omega)$ in the whole region $-\pi \le \omega < \pi$, i.e.,

$$\underset{\{g_m\}}{\operatorname{argmin}} \left\{ \int_{-\pi}^{\pi} \left(\sum_{m=-k}^{k} g_m e^{im\omega} - z(\omega) \right)^2 d\omega \right\} \tag{14}$$

subject to $f(0) = 0$. First, note the following theorem.

Theorem 2: If the $z(\omega)$ is an even (real) function, e.g., $-\omega^2$, then the coefficients will be symmetric, i.e., $g_m = g_{-m}$.

Proof of Theorem 2: Using a Lagrange multiplier to enforce the constraint $f(0) = 0$ [46], we find the following unconstrained optimization problem:

$$\underset{\{g_m\},\lambda}{\operatorname{argmin}} \left\{ \int_{-\pi}^{\pi} \left(\sum_{m=-k}^{k} g_m e^{im\omega} - z(\omega) \right)^2 d\omega + \lambda \sum_{m=-k}^{k} g_m \right\}. \tag{15}$$

Taking the partial derivative w.r.t. to $\{g_m\}$ and λ, and then letting the results all be zero, we find

$$g_m = c_m - \frac{\lambda}{4\pi} \quad (\text{for } m = -k, \ldots, k) \tag{16}$$

where $\{c_m\}$ are *Fourier transform* coefficients of $z(\omega)$, i.e.,

$$c_m = \frac{1}{2\pi}\int_{-\pi}^{\pi} z(\omega) e^{im\omega} d\omega. \tag{17}$$

If $z(\omega)$ is an even (real) function, then $\{c_m\}$ can be further written as *cosine transform* coefficients of $z(\omega)$, i.e.,

$$c_m = \frac{1}{\pi}\int_{0}^{\pi} z(\omega)\cos(m\omega) d\omega. \tag{18}$$

Note that $c_m = c_{-m}$, thus, $g_m = g_{-m}$. ■

Substitute (16) into the first equation in (11), we find

$$\lambda = \frac{4\pi}{2k+1}\sum_{m=-k}^{k} c_m. \tag{19}$$

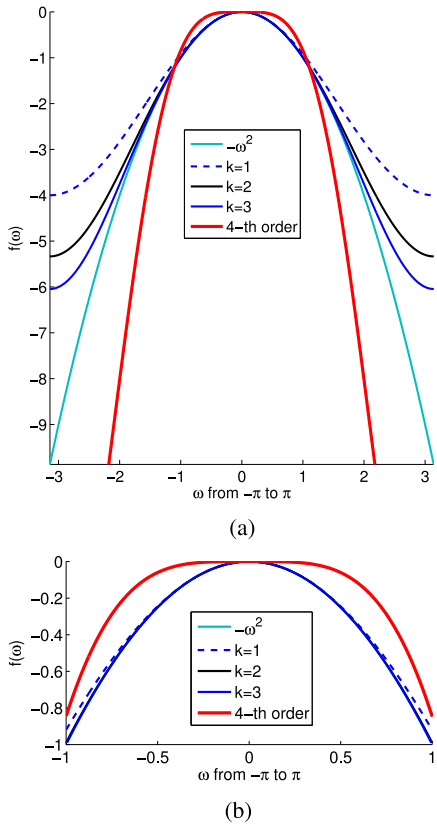

Fig. 3. Curves of $f(\omega)$ for the coefficients generated by Taylor series approach when $k=1,2,3$. Also shown is the red curve corresponds to the fourth-order coefficients $\{-1, 4, -6, 4, -1\}$, i.e., the Taylor series approximation of the polynomial $-\omega^4$. It is much "flatter" when $|\omega|$ is small. (a) Curves of various schemes. (b) Central area of the curves in (a).

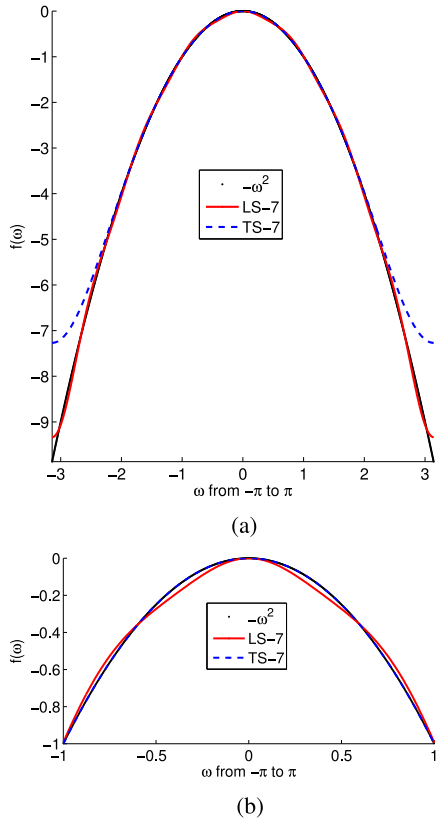

Fig. 4. Least-squares result (LSS-7) approximates $-\omega^2$ "globally." The Taylor series results (TS-7) approaches $-\omega^2$ much closer in the local region where $|\omega|$ is small. (a) Curves for different schemes. (b) Central area of the curves in (a).

Finally, we find the least-square solution

$$g_m = g_{-m} = c_m - \frac{1}{2k+1}\sum_{n=-k}^{k} c_n. \tag{20}$$

The remaining task is to choose an (even) objective function $z(\omega)$. The first choice is to let $z(\omega) = -\omega^2$. Correspondingly

$$c_m = \begin{cases} -\pi^2/3, & \text{if } m = 0 \\ (-1)^{|m|-1}2/m^2, & \text{otherwise} \end{cases}. \tag{21}$$

Fig. 4 shows the $f(\omega)$ (denoted by LSS-7) when $k = 7$. The 15 coefficients are: 0.0385, -0.0579, 0.0777, -0.1273, 0.2199, -0.5023, 1.9977, -3.2922, 1.9977, -0.5023, 0.2199, -0.1273, 0.0777, -0.0579, 0.0385. As a comparison, we also draw $f(\omega)$ obtained by the Taylor series approach[8] (denoted by TS-7). Unsurprisingly, the least-squares result approaches the curve $-\omega^2$ "globally," whereas the Taylor series for $-\omega^2$ is a better fit in the local region where $|\omega|$ is small [see Fig. 4(b)]. Moreover, the constraints in (11) imply that the three coefficients (when $k = 1$) will always be $\{1, -2, 1\}$ (up to a scale factor) no matter which approach is used.

[8]The coefficients by Taylor series approach (when $k = 7$) are: 0.00001, -0.00023, 0.00212, -0.01326, 0.06481, -0.29167, 1.75, -3.02359, 1.75, -0.29167, 0.06481, -0.01326, 0.00212, -0.00023, 0.00001. Note that some coefficients are too small to be used in real applications.

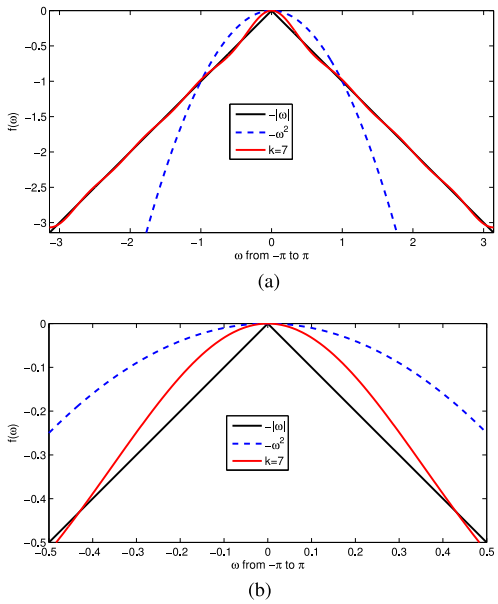

Fig. 5. Least-squares result (when $k = 7$) approximates $-|\omega|$ "globally." However, $f(\omega)$ cannot equal the "sharp corner" of $-|\omega|$ near $\omega = 0$. Outside that region (e.g., $0.1 < |\omega| < 0.5$), $f(\omega)$ drops much faster than $-\omega^2$. (a) Curve when $k = 7$. (b) Central of the curves in (a).

For the least-squares approach, we can try to approximate other nonpositive functions of ω, e.g., $-|\omega|$, which suppress low-frequency waves more efficiently. From (17), we find

$$c_m = \begin{cases} -\pi/2, & \text{if } m = 0 \\ (1-(-1)^{|m|})/(\pi m^2), & \text{otherwise} \end{cases}. \tag{22}$$

Fig. 5 shows the $f(\omega)$ (when $k = 7$) by least-squares approximation of $-|\omega|$. The 15 coefficients are: 0.0183, 0.0053, 0.0307, 0.0053, 0.0760, 0.0053, 0.6419, -1.5655, 0.6419, 0.0053, 0.0760, 0.0053, 0.0307, 0.0053, 0.0183. As discussed in Section III-B1, when $\omega \to 0$, the lowest-order polynomial that $f(\omega)$ can approach is $-\omega^2$. Thus, $f(\omega)$ cannot have the "sharp corner" of the curve $-|\omega|$. However, outside that neighborhood, e.g., when $0.1 < |\omega| < 0.5$, $f(\omega)$ drops much faster than $-\omega^2$, and approximates $-|\omega|$ well (see Fig. 5).

Note that $-\omega^2$ is larger than $-|\omega|$ when $1 < |\omega| < \pi$. Thus, another choice is to let $z(\omega) = \min\{-|\omega|, -\omega^2\}$, which is a continuous piecewise polynomial function. Correspondingly

$$c_m = (-1)^{|m|-1}\frac{2}{m^2} + \frac{1+\cos(m)}{\pi m^2} - \frac{2\sin(m)}{\pi m^3} \tag{23}$$

when $m \neq 0$, and $c_0 = -\pi^2/3 - 1/(6\pi)$.

Fig. 6 shows the result when $k = 7$. The 15 coefficients are: 0.0536, -0.0348, 0.1038, -0.1080, 0.2218, -0.5233, 1.9572, -3.3403, 1.9572, -0.5233, 0.2218, -0.1080, 0.1038, -0.0348, 0.0536. When $|\omega| \leq 1$, $f(\omega)$ approaches $|\omega|$, whereas when $1 < |\omega| \leq \pi$, $f(\omega)$ approaches $-\omega^2$. Of course, $f(\omega)$ still cannot have the "sharp corner" of $z(\omega)$ (at $\omega = 0$).

In summary, the two natural ways of extending traditional BCM, i.e., Taylor series and least-squares approximation of $-\omega^2$, will in effect *not* improve the BCM. In order to suppressing low-frequency components more efficiently, $z(\omega)$ should

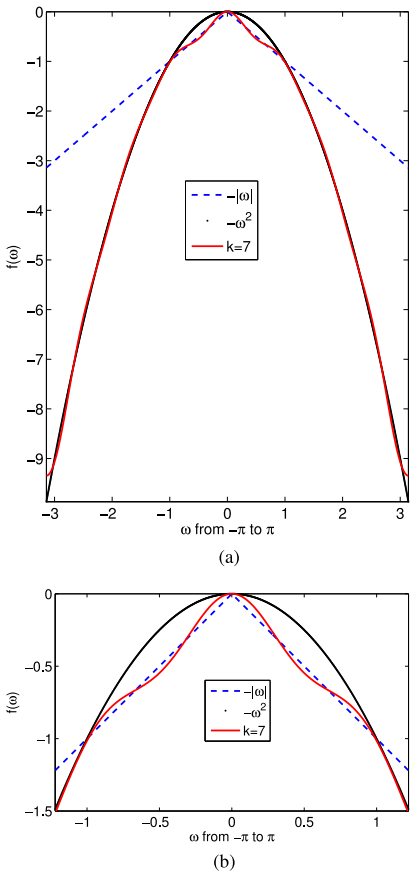

Fig. 6. Least-squares result (when $k = 7$) approximates $z(\omega)$ "globally." When $|\omega| \leq 1$, $f(\omega)$ "tries to" approach $|\omega|$, whereas when $1 < |\omega| \leq \pi$, $f(\omega)$ approaches $-\omega^2$. (a) Curve when $k = 7$. (b) Central area of the curves in (a).

be chosen to decay faster when $|\omega|$ is small, e.g., $-|\omega|$, such that smaller $f(\omega)$ (when $|\omega|$ is small) can be achieved by least-squares approximation. Note that Taylor series approach does not work in this case because $-|\omega|$ is *not* differentiable at $\omega = 0$, and $-\omega^2$ is the best choice for Taylor series approach.

IV. Testing Stability of the Coefficients

Although the functions approximated by $f(\omega)$, i.e., $-\omega^2$, $-|\omega|$, and $\min\{-|\omega|, -\omega^2\}$, are all negative when $0 < |\omega| \leq \pi$, we still need to verify the stability condition in Theorem 1. We provide conditions for checking stability of the generated coefficients, and then use them to test the coefficients obtained by the approaches introduced in this paper.

First, by (11) and the symmetry of $\{g_m\}$ (i.e., $g_m = g_{-m}$), we can rewrite $f(\omega)$ in (8) as

$$f(\omega) = -4 \sum_{m=1}^{k} g_m \sin^2\left(\frac{m\omega}{2}\right). \tag{24}$$

Equation (24) implies the following sufficient condition directly.

Theorem 3: If $g_m \geq 0$ for all $m = 1, 2, \ldots k$, and $g_0 < 0$, then the (symmetric) MN-BCM is stable.

The simplest bilateral control (1)—in which $k = 1$, $g_1 = 1$, and $g_0 = -2$—is stable. Moreover, we can prove the following.

Proposition 1: The symmetric MN-BCM whose coefficients are selected by least-squares approximation of $-|\omega|$ is stable.

Proof of Proposition 1: First, $c_m \geq 0$ for all $m \neq 0$ [see (22)]. Moreover, $\sum_{n=-k}^{k} c_n < 0$ (note that $\sum_{n=-\infty}^{\infty} c_n = 0$). Thus, $g_m > 0$ for all $m \neq 0$ [by (20)]. ■

For other schemes, g_m alternatingly has positive and negative signs [see, e.g., (21)]. It is not straightforward to "see" the sign of $f(\omega)$ in (24) directly. The (even) function $z(\omega)$ should match the stability condition in Theorem 1. We suggest that $z(\omega)$ be designed such that 1) $z(\omega) = 0$, and 2) $z(\omega)$ is decreasing when $0 \leq \omega \leq \pi$. All the functions $-\omega^2$, $-|\omega|$, and $\min\{-|\omega|, -\omega^2\}$ satisfy such conditions. For such $z(\omega)$, we should check the neighborhood around $\omega = 0$. Thus, a necessary (not sufficient) condition for testing stability is as follows.

Theorem 4: If the (symmetric) coefficients $\{g_m\}$ make MN-BCM stable, then they must satisfy the following condition:

$$G_k = \sum_{m=1}^{k} g_m m^2 > 0. \tag{25}$$

Proof of Theorem 4: From (24), we find that the first derivative of $f(\omega)$ is zero when $\omega = 0$. Thus, the condition $f(0) < 0$ for small $|\omega|$ requires

$$\left.\frac{d^2 f(\omega)}{d\omega^2}\right|_{\omega=0} < 0. \tag{26}$$

Substituting (24), we find (25). ■

For the scheme by Taylor series approximation of $-\omega^2$, the condition (26) is satisfied. The second derivative of $f(\omega)$ when $\omega = 0$ is -2 [see (12) and (13)]. Thus, (25) is also satisfied automatically. Moreover, we can prove the following.

Proposition 2: Coefficients generated by least-squares approximation of $-\omega^2$ satisfy the condition (25) in Theorem 4.

Proof of Proposition 2: Substituting (20) and (21) into (25), we can find:[9]

$$G_k = 2 \sum_{m=1}^{k} (-1)^{m-1} + C_k R_{k+1} \tag{27}$$

$$= \begin{cases} C_k R_{k+1}, & k \text{ is even} \\ 2 - 2C_k/(k+1)^2 + C_k R_{k+2}, & k \text{ is odd} \end{cases} \tag{28}$$

where

$$C_k = \frac{2}{2k+1}\left(\sum_{m=1}^{k} m^2\right) < k^2 \tag{29}$$

and (with odd k)

$$R_k = \sum_{m=k}^{\infty} c_m = \sum_{m=\frac{k+1}{2}}^{\infty} \left(\frac{2}{(2m-1)^2} - \frac{2}{(2m)^2}\right). \tag{30}$$

Note that $2 - 2C_k/(k+1)^2 > 0$ and R_k is *positive* when k is an odd number. Thus, G_k in (28) is positive. ■

[9]Note that $\sum_{m=1}^{\infty} 1/m^2 = \pi^2/6$ (see [47]). Thus, $\sum_{m=-\infty}^{\infty} c_m = 0$. Moreover, the sequence $\{c_m\}$ is absolute convergent. Thus, $\sum_{m=-k}^{k} c_m = -2\sum_{m=k+1}^{\infty} c_m$.

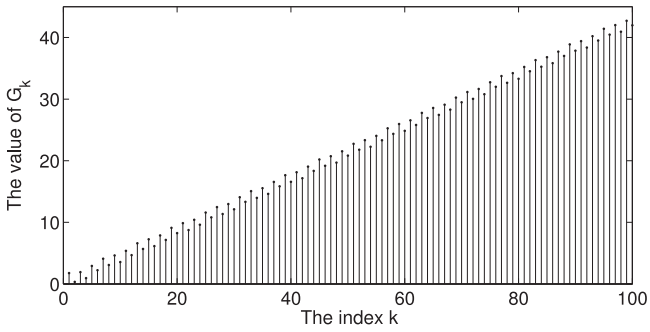

Fig. 7. Test of condition (25) for the coefficients generated by least-squares approximation of the function $\min\{-|\omega|, -\omega^2\}$. All the G_k (for k from 1 to 100) are positive numbers.

Proposition 3: Coefficients generated by least-squares approximation of $\min\{-|\omega|, -\omega^2\}$ satisfy the condition (25).

Proof of Proposition 3: First, calculate all G_k for some finite large k. Fig. 7 shows $\{G_k\}$ for $k = 1, 2, \ldots, 100$. They are all positive. The smallest value is 0.3365 (when $k = 2$).

Note that the term $-2\sin(m)/(\pi m^3)$ is negligible relative to other two terms in (23) for large m. Moreover, the term $(1 + \cos(m))/(\pi m^2)$ in (23) is positive. Thus, when m is large, the c_m in (23) is larger than the c_m in (21). That is, when k is large, the G_k corresponding to the least-squares approximation of $\min\{-|\omega|, -\omega^2\}$ will be larger than the G_k corresponding to the least-squares approximation of $-\omega^2$. ■

The closed-form solution of the newly designed $z(\omega)$, e.g., $e^{-\alpha|\omega|} - 1$ (with $\alpha > 0$) can be calculated directly using (18) and (20). Theorem 3 or Theorem 4 can then be used to check the corresponding results.

V. Simulations

We built a simulator with $N = 80$ cars running on a circular road. The car length was chosen to be $L = 5$ m. In the beginning, the space between successive cars was chosen to be a random number in the range from 23 to 27 m (with uniform distribution), with an average of 25 m. The initial speed of the cars was chosen as a random number between 23 and 27 m/s (with uniform distribution), with the average initial speed of 25 m/s. The car's density, i.e., the number of cars per mile (or per 1609.334 m), is plotted. The density can be estimated locally using $\rho_n = 1609.334/(x_{n-1} - x_n)$. The parameters used in the simulations are listed in Table I.

In the beginning, the cars are approximately evenly spaced and moving at approximately the same speed [see Fig. 8(a)]. Under car-following control, typical "stop-and-go" traffic patterns appear pretty soon.[10] Fig. 8(b) shows the traffic flow after 40 s using car-following control. This disturbed traffic flow pattern is used as the initial condition for various bilateral control schemes. Fig. 8(c) shows the result of SBC (3 node) after 160 s, i.e., when $t = 200$ s. The traffic flow is improved very efficiently, because the traveling waves (particularly the high-frequency components) are damped quickly. However, $f(\omega)$ approaches $-\omega^2$ for small $|\omega|$ [see Fig. 3(b)]. Thus, the low-frequency components do *not* disappear as fast, and the traffic flow does *not* continue to approach the equilibrium state as efficiently as it did initially. As a comparison, Fig. 8(d) shows the results of 15 nodes bilateral control (i.e., $k = 7$). Here, the coefficients are obtained by least-squares approximation of $-|\omega|$ (denoted by LSA-7). The traffic flow goes to the equilibrium state much more efficiently. The corresponding $f(\omega)$ is smaller than $-\omega^2$ when $|\omega|$ is small [see Fig. 5(b)], i.e., the low-frequency waves are damped much more quickly.

TABLE I
Parameters Used in the Simulation

distance feedback k_d	0.1 (1/sec^2)
velocity feedback k_v	0.1 (1/sec)
Car length L	5 (meters)
max velocity $v_{\max}$	160 (km/h)
min velocity $v_{\min}$	0 (km/h)
max acceleration $a_{\max}$	5 (m/sec^2)
min deceleration $a_{\min}$	-5 (m/sec^2)
time step Δt	0.1 (sec)

The result of 15-node bilateral control (i.e., $k = 7$) whose coefficients obtained by Taylor series approach (denoted by TS-7) and the result of 15-node bilateral control whose coefficients obtained by least-squares approximation of $-\omega^2$ (denoted by LSS-7) look very similar to the result in Fig. 8(c). The result of 15-node bilateral control whose coefficients obtained by least-squares approximation of $\min\{-|\omega|, -\omega^2\}$ (denoted by LSZ-7) looks very similar to the result in Fig. 8(d). Note that as time goes on, high-frequency waves are damped away. The low-frequency waves matter; thus, the performance of TS scheme and LSS scheme is closer and closer to the performance of SBC scheme, whereas the performance of LSZ scheme will be closer and closer to the performance of LSA scheme. The simulation results and MATLAB codes are on our webpage http://people.csail.mit.edu/wangliang.

Fig. 9 shows the simulation results of the space between successive cars (including the car length L), i.e., $x_{n-1} - x_n$ or $d_n + L$. In the first 40 s, the traffic is under car-following control. After that, various bilateral control schemes are used. Fig. 9(a) and (b) looks very similar. Thus, Taylor series is not an efficient extension of the simplest BCM for damping the low-frequency perturbations. LSS-7 shows some improvement, but *not* very significant [see Fig. 9(c)]. Comparing to Fig. 9(d) and (e), we can see that LSA-7 and LSZ-7 have advantage of suppressing low-frequency fluctuation in $x_{n-1} - x_n$ (especially, when $t >$ 160 s). Fig. 9(f) shows the space $\{d_n + L\}$ of these five bilateral control schemes when $t = 180$ s. The fluctuation in the results by SBC and TS-7 is quite close, whereas the fluctuation in the results by LSA-7 and LSZ-7 is much smaller.

Here, we use the AAD

$$E_A(t) = \frac{1}{N}\sum_{n=1}^{N} |d_n(t) - s| \tag{31}$$

[10]We use constant-time headway model $a_n = k_d(d_n - v_n T) + k_v(v_{n-1} - v_n)$ with $T = 1$ s. The corresponding stability condition is [3], [4], [31]: $2k_v T + k_d T^2 > 2$. Thus, the traffic flow is unstable.

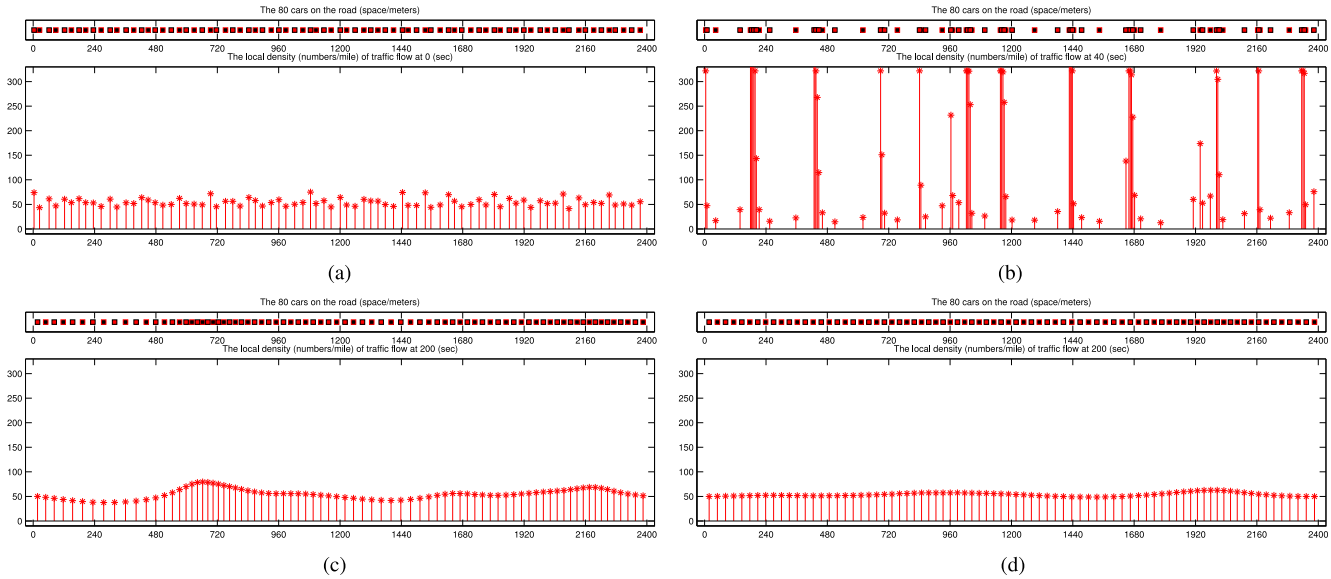

Fig. 8. Demonstration of traffic flow under various control schemes. (a) Traffic flow in the beginning is smooth. All the cars are approximately evenly spaced and move at approximately the same speed (The initial traffic condition for simulation). (b) Under car-following control, "stop-and-go" traffic patterns appear soon. From the initial condition in Fig. 8(b), various BCMs are used for 160 s (Car-following control after 40 s). (c) Result of the simplest (3 node) bilateral control (SBC) (SBC after 160 s). (d) Result of 15 nodes bilateral control with coefficients obtained by the least-squares approximation of $-|\omega|$ (LSZ-7 scheme after 160 s).

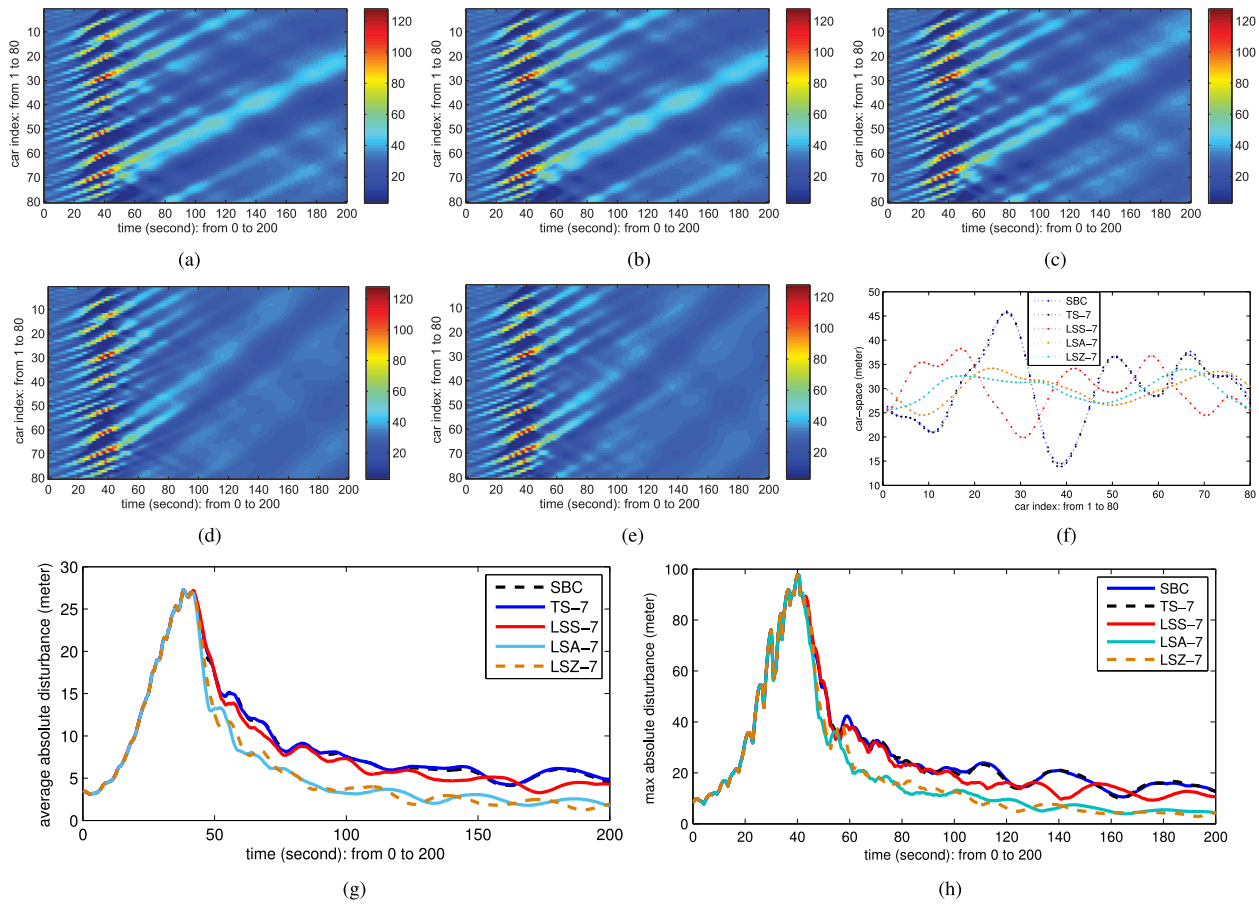

Fig. 9. Simulation of space $\{x_{n-1} - x_n\}$ between successive cars. The first 40 s is under car-following controlled. After then, various bilateral control schemes are used. The circular boundary condition is used for this simulation. The colors in (a)–(f) are shown in meters. (a) SBC. (b) Bilateral control by TS-7. (c) Bilateral control by LSS-7. (d) Bilateral control by LSA-7. (e) Bilateral control by LSZ-7. (f) Space $d_n + L$ when $t = 180$ s. (g) Average absolute disturbance (AAD). (h) Maximum absolute disturbance (MAD).

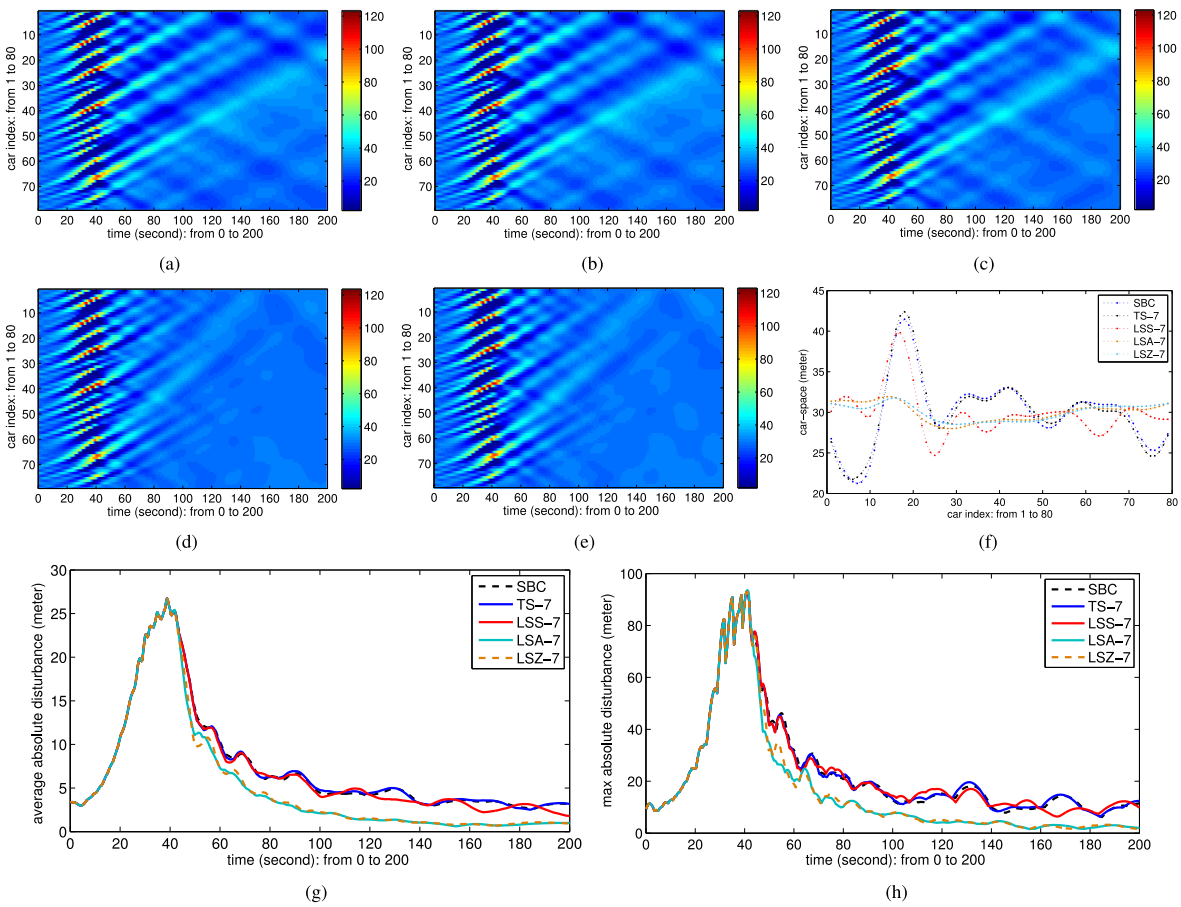

Fig. 10. Simulation of space $\{x_{n-1} - x_n\}$ between successive cars. The first 40 s is under car-following controlled. After then, various bilateral control schemes are used. The circular boundary condition is chosen as free–free. The colors in (a)–(f) are shown in meters. (a) SBC. (b) Bilateral control by TS-7. (c) Bilateral control by LSS-7. (d) Bilateral control by LSA-7. (e) Bilateral control by LSZ-7. (f) Space $d_n + L$ when $t = 200$ s. (g) AAD. (h) MAD.

and MAD

$$E_M(t) = \max_{n\in\{1,\ldots,N\}} \{\,|d_n(t) - s|\} \tag{32}$$

to evaluate the fluctuation in the result. Fig. 9(g) and (h) shows the AAD and MAD of the simulation results in Fig. 9. Still, the results of SBC and TS-7 are very similar. The results of LSA-7 and LSZ-7 are smaller than other schemes when, e.g., $t > 60$ s. At $t = 200$ s, the AAD and MAD of the results of LSA-7 and LSZ-7 are both smaller than the corresponding values in the very beginning (i.e., $t = 0$). However, the AAD and MAD of the results of other three bilateral control schemes are both larger than the corresponding values in the very beginning.

We also did the simulation with free–free boundaries. Note that different from platooning, there are no "leaders" in bilateral control; thus, it is more natural to use free–free boundaries, rather than fixed–free boundaries used in platooning [13], [38]. The initial settings are the same as the experiments with circular boundaries (see Table I). The traffic is under car-following control in the first 40 s, which cause the "stop-and-go" instabilities. After that, various bilateral control schemes are used to suppress traffic flow instabilities. Fig. 10 shows the simulation results. Similar to the results in Fig. 9, traffic flow instabilities are suppressed by bilateral control. Moreover, LSA-7 and LSZ-7 schemes suppress fluctuation of the space between successive cars much more efficiently.

Fig. 11 shows more experimental results. Fig. 11(a)–(c) shows the results when $k = 3$. Note that $f(\omega)$ does not approximate the objective curves, e.g., $-|\omega|$ well when k is relatively small. Thus, the low-frequency fluctuation is not damped very efficiently, and the performance of the three least-squares approaches, i.e., LSS-3, LSA-3, and LSZ-3, is close. However, LSS-3, LSA-3, and LSZ-3 are still shown to be more efficient extension of SBC than the Taylor series approach (TS-3). Unsurprisingly, as k increases, $f(\omega)$ approaches the corresponding objective curve better and better. Fig. 11(d)–(f) shows the extreme case of large $k = 21$. The corresponding $f(\omega)$ of LSS-21 and TS-21 is almost the same when ω is small. Thus, the performance of LSS-21 and TS-21 is similar, which is close to the performance of the SBC. Moreover, the advantage of damping low-frequency waves by LSA-7 and LSZ-7 becomes more obvious. All the initial settings are the same as the one used in the simulation with circular boundaries.

We also did the simulation when the measurements contain noise. Fig. 11(g)–(i) shows the results. The initial settings are the same as the one used in the simulation with free–free boundaries. The distance measurement of every car in each iteration

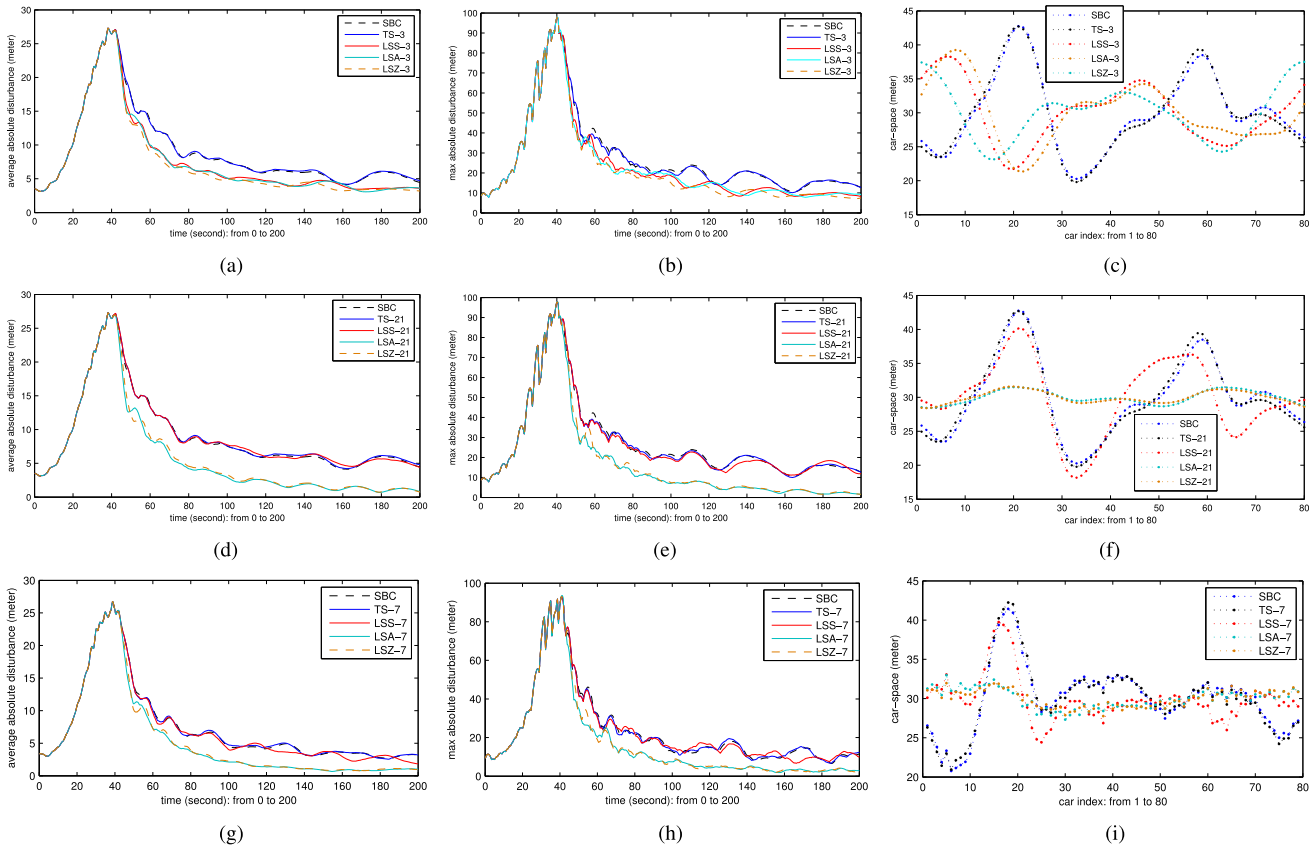

Fig. 11. More simulation results. (a)–(c) Results with small $k = 3$. The low-frequency fluctuation is not damped effectively by LSA-3 and LSZ-3. (d)–(f) Results with large $k = 21$. The low-frequency fluctuation is damped more effectively by LSA-21 and LSZ-21. The performance of LSS-21 is more similar to the performance of TS-21 and SBC. (g)–(i) Simulation results when additional measurement errors are included. These results look close to the corresponding ones shown in Fig. 10 (with small additional noise). The bilateral control schemes are still stable. (a) AAD (when $k = 3$). (b) MAD (when $k = 3$). (c) Space at $t = 200$ s (when $k = 3$). (d) AAD (when $k = 21$). (e) MAD (when $k = 21$). (f) Space at $t = 200$ s (when $k = 21$). (g) AAD (when $k = 7$). (h) MAD (when $k = 7$). (i) Space at $t = 200$ s (when $k = 7$).

has a random value between -2 and 2 m added to it. The velocity measurement of every car in each iteration also has a random value between -1 and 1 m/s added to it. These noisy measurements are then used to calculate the acceleration commanded by the car. The simulation results look like the results in Fig. 10 with small additional noise. Fig. 11(g) and (h) shows the AAD and MAD of the results, respectively. They look close to the results in Fig. 10(g) and (h). Fig. 11(i) shows the space $\{x_{n-1} - x_n\}$ between successive cars when $t = 200$ s, which basically looks like the result in Fig. 10(f) with some additional noise.

In summary, the simulations validate the analysis in Section III. Neither Taylor series approach nor least-squares approximation of $-\omega^2$ can improve traditional BCM effectively. In contrast, least-squares approximation of $-|\omega|$ or $\min\{-\omega^2, -|\omega|\}$ provides an effective way to damp low-frequency fluctuation much faster, and thus should be used in real applications.

VI. Conclusion

Traditional bilateral control uses sensors in the controlled vehicle to determine the relative position and relative velocity of the leading and following vehicles. Using wireless communication, information about the state of cars other than just the immediately leading and following cars can be made available to the longitudinal control algorithm. This makes it possible to extend the traditional 3-node bilateral control. In this paper, we provide one such model that we call "multinode bilateral control." One basic problem of the MN-BCM is how to suppress traffic flow instabilities more efficiently by assigning weights (or coefficients) for the additional measurements. By stability analysis, we show that the objective of picking coefficients is (roughly speaking) to "suppress low-frequency perturbation-caused wave more effectively." That is, to make $f(\omega)$ in (8) as small as possible by picking the coefficients $\{g_m\}$ in (8).

We explore two different approaches—the Taylor series approach and the least-squares approach—to generate coefficients for the multinode bilateral control strategy. We show that the two natural ways of extending traditional BCM, i.e., Taylor series and least-squares approximation of $-\omega^2$ *cannot* improve BCM effectively. The best that the Taylor series approach can do is to approximate $-\omega^2$. Thus, the Taylor series approach cannot be used to improve the BCM effectively. However, a least-square approach *does* provide an effective way to improving BCM—by carefully designing the function $z(\omega)$. In order to suppressing low-frequency components more efficiently, $z(\omega)$ should be designed to decay faster when $|\omega|$ is small, e.g., $-|\omega|$ or $\min\{-\omega^2, -|\omega|\}$. Simulation results confirm our analysis.

Thus, we suggest the use of results obtained by least-squares approximation of $-|\omega|$ or $\min\{-\omega^2, -|\omega|\}$ in real applications.

Note that $z(\omega)$ can be chosen to have other forms e.g., $e^{-\alpha|\omega|} - 1$ (with $\alpha > 0$). We suggest that the even function $z(\omega)$ should be designed such that 1) $z(0) = 0$, 2) be nonincreasing when $0 \leq \omega \leq \pi$, and 3) decay much faster than $-\omega^2$ when $|\omega|$ is small (e.g., with "sharp corner" at $\omega = 0$). We give the close-form solution of the least-squares approach, i.e., (18) and (20), and also provide both sufficient (see Theorem 3) and necessary (see Theorem 4) conditions for checking the stability of new results. This makes it possible to easily calculate the coefficients for a newly designed $z(\omega)$.

Bilateral control uses symmetric coefficients. The stability condition is in Theorem 1. However, if the coefficients are not symmetric (e.g., when the desired space from the leading car is emphasized more than the desired space from tailing car), then $f(\omega)$ will contain imaginary parts. Now, the stability condition—the real parts of the two roots s_1 and s_2 solved from (10) are both nonpositive—will *not* be so simple. The paper presented in [38] gives mathematical analysis of the three-node asymmetric case. Some mathematical technics used in the platoon models are helpful to analyze the multinode cases [32]–[37].

In this paper, we choose $g_m = h_m$. Otherwise, the stability condition in Theorem 1 should be satisfied by both $\{g_m\}$ and $\{h_m\}$ [see (10)]. One future exploration is how to improve MN-BCM further by picking different set of gains $\{g_m\}$ and $\{h_m\}$. Although the traffic purely under car-following control, or purely under bilateral control, is similar to some special cases of decentralized platooning, here, we should mention that both car-following control and bilateral control are only applied to a single vehicle, and thus, there is *no* such requirement that all the vehicles are under the same control strategy. In our future work, we will study such mixed traffic.

ACKNOWLEDGMENT

The authors would like to acknowledge the helpful discussions with Prof. G. Strang about the mathematical analysis. The authors would also want to thank the good suggestions from the reviewers.

REFERENCES

[1] B. K. P. Horn, "Suppressing traffic flow instabilities," in *Proc. IEEE Int. Conf. Intell. Transp. Syst.*, 2013, pp. 13–20.
[2] T. Baran and B. K. P. Horn, "A robust signal-flow architecture for cooperative vehicle density control," in *Proc. IEEE Int. Conf. Acoust., Speech, Signal Process.*, 2013, pp. 2790–2794.
[3] L. Wang, B. K. P. Horn, and G. Strang, "Eigenvalue and eigenvector analysis of stability for a line of traffic," *Stud. Appl. Math.*, vol. 138, no. 1, pp. 103–132, 2017.
[4] B. K. P. Horn and L. Wang, "Wave equation of suppressed traffic flow instabilities," *IEEE Trans. Intell. Transp. Syst.*, vol. 19, no. 9, pp. 2955–2964, Sep. 2018. [Online]. Available: http://ieeexplore.ieee.org/document/8166801
[5] A. Nakayama, Y. Sugiyama, and K. Hasebe, "Effect of looking at the car that follows in an optimal velocity model of traffic flow," *Phys. Rev. E*, vol. 65, no. 1, 2001, Art. no. 016112.
[6] M. Treiber and D. Helbing, "Hamilton-like statistics in onedimensional driven dissipative many-particle systems," *Eur. Phys. J. B*, vol. 8, no. 4, pp. 607–618. 2009.
[7] C. C. Chien, Y. Zhang, and C. Y. Cheng, "Autonomous intelligent cruise control using both front and back information for tight vehicle following maneuvers," in *Proc. IEEE Amer. Control Conf.*, 1995, pp. 3091–3095.
[8] W. S. Levine and M. Athans, "On the optimal error regulation of a string of moving vehicles," *IEEE Trans. Autom. Control*, vol. AC-11, no. 3, pp. 355–361, Jul. 1966.
[9] S. Sheikholeslam and C. A. Desoer, "Longitudinal control of a platoon of vehicles," in *Proc. IEEE Amer. Control Conf.*, 1990, pp. 291–296.
[10] P. Varaiya, "Smart cars on smart roads: Problems of control," *IEEE Trans. Autom. Control*, vol. 38, no. 2, pp. 195–207, Feb. 1993.
[11] D. N. Godbole and J. Lygeros, "Longitudinal control of the lead car of a platoon," *IEEE Trans. Veh. Technol.*, vol. 43, no. 4, pp. 1125–1135, Nov. 1994.
[12] S. S. Stanković, M. J. Stanojevic, and D. D. Siljak, "Decentralized overlapping control of a platoon of vehicles," *IEEE Trans. Control Syst. Technol.*, vol. 8, no. 5, pp. 816–832, Sep. 2000.
[13] P. Barooah and J. P. Hespanha, "Error amplification and disturbance propagation in vehicle strings with decentralized linear control," in *Proc. IEEE Conf. Decis. Control*, 2005, pp. 4964–4969.
[14] P. Barooah, M. G. Prashant, and J. P. Hespanha, "Mistuning-based control design to improve closed-loop stability margin of vehicular platoons," *IEEE Trans. Autom. Control*, vol. 54, no. 9, pp. 2100–2113, Sep. 2009.
[15] H. He, P. Barooah, and P. G. Mehta, "Stability margin scaling laws for distributed formation control as a function of network structure," *IEEE Trans. Autom. Control*, vol. 56, no. 4, pp. 923–929, Apr. 2011.
[16] F. Lin, M. Fardad, and M. R. Jovanović, "Optimal control of vehicular formations with nearest neighbor interactions," *IEEE Trans. Autom. Control*, vol. 57, no. 9, pp. 2203–2218, Sep. 2012.
[17] R. H. Middleton and J. H. Braslavsky, "String instability in classes of linear time invariant formation control with limited communication range," *IEEE Trans. Autom. Control*, vol. 55, no. 7, pp. 1519–1530, Jul. 2010.
[18] M. R. Jovanović and B. Bamieh, "Lyapunov-based distributed control of systems on lattices," *IEEE Trans. Autom. Contol*, vol. 50, no. 4, pp. 422–433, Apr. 2005.
[19] M. R. Jovanović and B. Bamieh, "On the ill-posedness of certain vehicular platoon control problems," *IEEE Trans. Autom. Control*, vol. 50, no. 9, pp. 1307–1321, Sep. 2005.
[20] M. R. Jovanović, J. M. Fowler, B. Bamieh, and R. D'Andrea, "On the peaking phenomenon in the control of vehicular platoons," *Syst. Control Lett.*, vol. 57, no. 7, pp. 528–537, 2008.
[21] B. Bamieh, M. R. Jovanović, P. Mitra, and S. Patterson, "Coherence in large-scale networks: Dimension-dependent limitations of local feedback," *IEEE Trans. Autom. Control*, vol. 57, no. 9, pp. 2235–2249, Sep. 2012.
[22] A. Uno, S. Takeshi, and T. Sadayuki Tsugawa , "A merging control algorithm based on inter-vehicle communication," in *Proc. IEEE Int. Conf. Intell. Transp. Syst.*, 1999, pp. 783–787.
[23] B. Ran, S. Leight, and B. Chang, "A microscopic simulation model for merging control on a dedicated-lane automated highway system," *Transp. Res. Part C*, vol. 7, no. 6, pp. 369–388, 1999.
[24] S. Hallé and B. Chaib-draa , "A collaborative driving system based on multiagent modelling and simulations," *Transp. Res. Part C*, vol. 13, no. 4, pp. 320–345, 2005.
[25] P. Seiler, A. Pant, and K. Hedrick, "Disturbance propagation in vehicle strings," *IEEE Trans. Autom. Control*, vol. 49, no. 10, pp. 1835–1842, Oct. 2004.
[26] M. E. Khatir and J. D. Edward, "Decentralized control of a large platoon of vehicles using non-identical controllers," in *Proc. IEEE Amer. Control Conf.*, 2004, pp. 2769–2776.
[27] L. Peppard, "String stability of relative-motion PID vehicle control systems," *IEEE Trans. Autom. Control*, vol. AC-19, no. 5, pp. 579–581, Oct. 1974.
[28] D. Swaroop and J. K. Hedrick, "String stability of interconnected systems," *IEEE Trans. Autom. Control*, vol. 41, no. 3, pp. 349–357, Mar. 1996.
[29] J. Ploeg, N. V. D. Wouw, and H. Nijmeijer, "L_p string stability of cascaded systems: Application to vehicle platooning," *IEEE Trans. Control Syst. Technol.*, vol. 22, no. 2, pp. 786–793, Mar. 2014.
[30] S. Elaine and J. K. Hedrick, "String stability analysis for heterogeneous vehicle strings," in *Proc. IEEE Amer. Control Conf.*, 2007, pp. 3118–3125.
[31] L. Wang and B. K. P. Horn, "Time-to-contact control for safety and reliability of self-driving cars," in *Proc. IEEE Int. Smart Cities Conf.*, 2017, pp. 1–4.
[32] S. E. Li, Y. Zheng, K. Li, and J. Wang, "An overview of vehicular platoon control under the four-component framework," in *Proc. IEEE Intell. Veh. Symp.*, 2015, pp. 286–291.

[33] Y. Zheng, S. E. Li, K. Li, and L. Wang, "Stability margin improvement of vehicular platoon considering undirected topology and asymmetric control," *IEEE Trans. Control Syst. Technol.*, vol. 24, no. 4, pp. 1253–1265, Jul. 2016.
[34] Y. Zheng, S. E. Li, J. Wang, D. Cao, and K. Li, "Stability and scalability of homogeneous vehicular platoon: Study on the influence of information flow topologies," *IEEE Trans. Intell. Transp. Syst.*, vol. 17, no. 1, pp. 14–26, Jan. 2016.
[35] Y. Zheng, S. E. Li, K. Li, and W. Ren, "Platooning of connected vehicles with undirected topologies: Robustness analysis and distributed H-infinity controller synthesis," *IEEE Trans. Intell. Transp. Syst.*, vol. 19, no. 5, pp. 1353–1364, May 2018.
[36] S. E. Li, X. Qin, K. Li, J. Wang, and B. Xie, "Robustness analysis and controller synthesis of homogeneous vehicular platoons with bounded parameter uncertainty," *IEEE/ASME Trans. Mechatronics*, vol. 22, no. 2, pp. 1014–1025, Apr. 2017.
[37] S. Stdli, M. M. Seron, and R. H. Middleton, "Vehicular platoons in cyclic interconnections," *Automatica*, vol. 94, pp. 283–293, 2018.
[38] H. Hao and P. Barooah, "On achieving size-independent stability margin of vehicular lattice formations with distributed control," *IEEE Trans. Autom. Control*, vol. 57, no. 10, pp. 2688–2694, Oct. 2012.
[39] I. Herman, D. Martinec, Z. Hurák, and M. Šebek, "Nonzero bound on Fiedler eigenvalue causes exponential growth of H-infinity norm of vehicular platoon," *IEEE Trans. Autom. Control*, vol. 60, no. 8, pp. 2248–2253, Aug. 2015.
[40] D. Martinec, I. Herman, and M. Šebek, "On the necessity of symmetric positional coupling for string stability," *IEEE Trans. Control Netw. Syst.*, vol. 5, no. 1, pp. 45–54, Mar. 2018.
[41] C. K. Verginis, C. P. Bechlioulis, D. V. Dimarogonas, and K. J. Kyriakopoulos, "Robust distributed control protocols for large vehicular platoons with prescribed transient and steady-state performance," *IEEE Trans. Control Syst. Technol.*, vol. 26, no. 1, pp. 299–304, Jan. 2018.
[42] G. Strang, *Introduction to Linear Algebra*. Wellesley, MA, USA: Wellesley-Cambridge Press, 2016.
[43] G. Strang, *Computational Science and Engineering*. Wellesley, MA, USA: Wellesley-Cambridge Press, 2007.
[44] L. R. Turner, "Inverse of the Vandermonde matrix with applications," Nat. Aeronaut. Space Admin., Washington, DC, USA, NASA Tech. Note D-3547, 1966.
[45] H. Oruç and G. M. Phillips, "Explicit factorization of the Vandermonde matrix," *Linear Algebra Appl.*, vol. 315, no. 1, pp. 113–123, 2000.
[46] B. K. P. Horn, *Robot Vision*. Cambridge, MA, USA: MIT Press, 1986, p. 463.
[47] I. S. Gradshteyn and I. M. Ryzhik, *Table of Integrals, Series, and Products*, 8th ed. New York, NY, USA: Elsevier, 2014 (Transl: from the Russian).

Liang Wang was born in 1983. He received the B.S. and M.S. degrees in electronic engineering from the School of Electronic and Information Engineering, Beijing Jiaotong University, Beijing, China, in 2006 and 2008, respectively, and the Ph.D. degree in computer and information technology from the School of Computer and Information Technology, Beijing Jiaotong University, in January 2015.

From September 2011 to March 2013, he was a Visiting Scholar with the Mathematics Department, Massachusetts Institute of Technology (MIT), Cambridge, MA, USA. From January 2015 to December 2018, he was a Postdoctoral Research Scholar with the Computer Science and Artificial Intelligence Laboratory, MIT. His research interests include machine vision, inverse problems, and intelligent vehicles.

Berthold K. P. Horn received the B.Sc.Eng. degree in electrical engineering from the University of the Witwatersrand, Johannesburg, South Africa, in 1965, and the S.M. and Ph.D. degrees in electronic engineering and computer science from Massachusetts Institute of Technology (MIT), Cambridge, MA, USA, in 1968 and 1970, respectively.

He is currently a Professor of Electrical Engineering and Computer Science with the MIT. He is the author, coauthor, or Editor of books on the programming language LISP and machine vision, including *Robot Vision* (MIT Press, 1986). His research interests include machine vision, computational imaging, and intelligent vehicles.

Dr. Horn was the recipient of the Rank Prize for pioneering work leading to practical vision systems in 1989 and was elected a Fellow of the American Association of Artificial Intelligence in 1990 for significant contributions to artificial intelligence. He was elected to the National Academy of Engineering in 2002 and was the recipient of the Azriel Rosenfeld Lifetime Achievement Award from the IEEE Computer Society for pioneering work in early vision in 2009.